Convolutional neural network augmented soft-sensor for autonomous microfluidic production of uniform bubbles

Owen Land[a], Warren D. Seider[a], Daeyeon Lee[a]

[a]*Department of Chemical and Biomolecular Engineering, University of Pennsylvania, Philadelphia, USA*

Keywords: droplets, control, artificial-intelligence, disturbance rejection

Abstract

Microfluidics has emerged as a foundational process for creating highly uniform emulsions and bubbles. To enable integration of microfluidic platforms into industrial processes, achieving precise control over the size uniformity of microfluidic-generated bubbles and emulsions is crucial. Even if the external variables such as flow rates or pressures are kept constant, microfluidic processes can be easily disturbed by unknown factors that would substantially compromise the uniformity of resulting emulsions and bubbles. In this study, we introduce a two-step soft-sensor approach that combines a convolutional neural network (CNN) and an image recognition algorithm for feature extraction to detect both the flow regime and the size and uniformity of resulting bubbles. By using the CNN to detect flow regimes, our controller is able to restore the bubble-producing flow regime in response to disturbances. Beyond self-recovery, our controller actively adjusts to minimize errors, maintain setpoints, mitigate disturbances, and ensure system stability over extended periods. 99.2% of bubbles produced during an 8-hour period remain within 5% of the setpoint with our controller taking action. By leveraging the soft sensor and artificial intelligence-assisted feedback control, our work presents a widely applicable approach for precise and automated control of microfluidics in diverse applications.

1. Introduction

Microfluidics enables the production and manipulation of multi-phasic mixtures such as gas bubbles, liquid droplets and multiple emulsions with unparalleled precision and control.

Leveraging advanced techniques in micro/nano-fabrication, precise microchannels can be manufactured to control droplets and bubbles for a wide range of advanced applications [1]. For example, chemical reactions can be induced in single droplets, providing a unique platform to conduct high-throughput analyses and synthesis with minimal reagents use and reduced waste [2–4]. Furthermore, droplet microfluidics facilitates the encapsulation of delicate biological materials such as cells and proteins under mild conditions that preserve their functionality and viability, which is particularly well-suited for the development of low-cost and highly efficient biomedical diagnostics and therapeutics [5–7]. The precision and scalability of droplet microfluidics enables fabrication of functional particles such as microbubbles, microcapsules and nanoparticles with precisely designed morphology and functionality, enhancing disease diagnostics as well as controlled release and targeted delivery of various pharmaceutical actives [8–10].

Achieving consistent uniformity in the production of droplets and bubbles throughout the operation of microfluidic devices is crucial for harnessing the full benefits of this technology. The maintenance of uniformity is, however, challenged by several factors, which necessitates continuous user intervention to adjust flow rates and pressures, ensuring that the droplet and bubble production maintains the desired dimensions and properties. Even seemingly negligible changes in operating conditions can cause large fluctuations in performance of device output because of the sensitivity of flow behaviors of fluids at the microscopic scale. Over time, the performance of microfluidic devices may be further compromised by issues such as surface fouling, changes in wetting properties, channel clogging and the solvent-induced swelling of the microfluidic devices [11–13]. These factors introduce additional layers of complexity in achieving and maintaining the uniformity of droplet and bubble generation, posing significant challenges to the scalability and reliability of microfluidic applications.

Developing autonomous microfluidic systems capable of self-adapting to changing conditions would enable the precise formation of a wide array of droplets and bubbles with complex composition and morphology without direct operator intervention [14]. The realization of such a capability will enhance the efficiency and effectiveness of droplet and bubble microfluidics and simultaneously lead to new applications that leverage the full potential of this versatile technology.

A few recent studies have demonstrated the ability to control droplet microfluidics, using technologies such as neural networks and reinforcement learning to gather insight on flow regimes in microfluidics over various flow conditions [15,16]. Other techniques involve the use of impedance electronics embedded into the microfluidic device as a sensor for measuring microbubble diameter as a function of the voltage measured or measuring the interference pattern created by focusing a laser on droplets in the outlet channel using piezoelectric transducer [17,18]. Vision Development Module within LabVIEW (National Instruments™) has been used for droplet detection and control using a virtual instrument [19]. In addition, feedback sensors have been developed for precise control of flowrates and pressures in microfluidic devices off-chip [20,21]. Despite these advances, many of these approaches use highly sophisticated sensing techniques that involve specialized equipment not traditionally used in microfluidics, do not have the ability to easily measure process variables on-chip, and do not have the ability to control the system when it is disturbed to reach different flow regimes, such as one in which bubbles or droplets are not produced.

In this study, we introduce an autonomous microfluidics system that relies simply on microscopic imaging and is trained with a convolutional neural network (CNN) to return the process to the desired microbubble production flow regime. Our system is able to control the size of microfluidic bubble production using only commercially available pressure controllers, a microscope, and a high-speed camera, all of which are commonly employed in microfluidic setups. We generate gas bubbles in a flow-focusing device by applying pressure to the dispersed gas phase using a high-pressure nitrogen canister. Additionally, we use pressure-driven flow, also from a high-pressure nitrogen canister, to pressurize a liquid reservoir, thereby pushing the liquid into the microfluidic chip. Pressure driven flow of the aqueous phase is chosen over commercially available syringe pumps because of their significantly reduced response times without periodic fluctuations [22]. Gas bubbles are selected over liquid droplets due to their greater size variability for various reasons including the compressibility of the gas phase, large interfacial tension, and significantly different viscosity of the two phases, necessitating enhanced control.

Our control system actively adjusts either the liquid driving pressure or gas pressure to ensure the bubbles being produced match the user-specified setpoint for the bubble diameter while showing effective setpoint tracking, disturbance rejection, and stability over an eight-hour period. Potentially, our approach can be trained to control the shape of particles produced by microfluidics such as rods and discs, and higher-order geometries such as double emulsions and Janus droplets.

2. Materials and Methods

2.1. Flow focusing generator for gas-bubble production

We use a well-established flow-focusing generator to produce gas bubbles [23,24]. This geometry splits the continuous phase into two streams which subsequently surround and pinch off the dispersed phase at a cross junction, as shown in Figure 1. The symmetry of the junction allows for more flexibility in the size and frequency of bubble generation. The immiscibility of the two phases forces bubbles to form through either a dripping or jetting mechanism [25]. The dripping regime involves the periodic breakup of a fluid stream into bubbles due to capillary instability. This instability arises from the interplay of surface tension and viscous forces. The dripping frequency is governed by the capillary number (Ca), representing the ratio of viscous to capillary forces. The jetting regime involves the stretching of a fluid stream into an extended jet due to the dominance of inertial forces or viscous forces over capillary forces. Microfluidic droplets and bubbles produced in the jetting regime are larger and less uniform compared to those formed in the dripping regime due to the unfixed interface position during breakup [26]. Controlling the flows of the two fluid phases to maintain microfluidic generation in the dripping regime is critical to maintaining the uniformity of resulting droplets and bubbles [27].

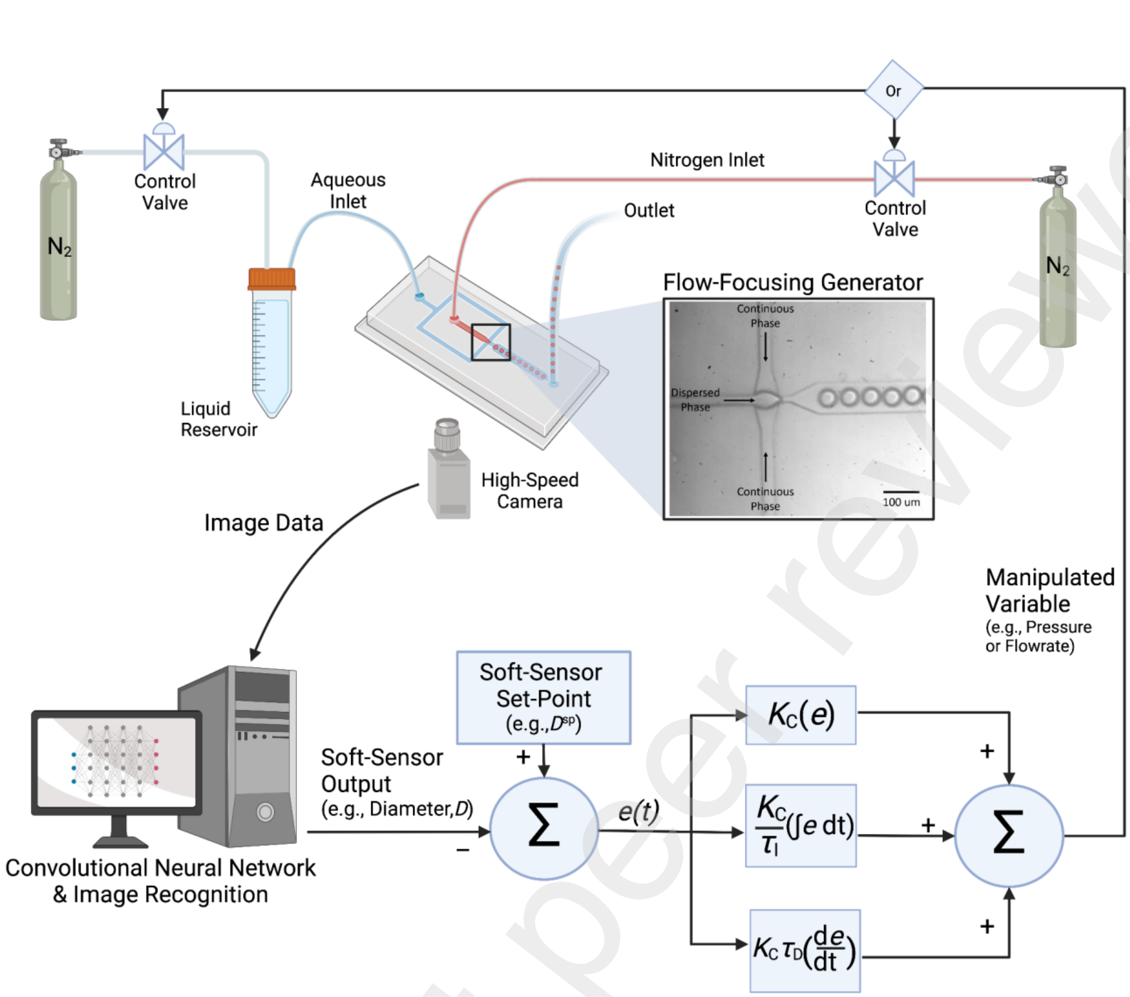

Figure 1. Control schematic using CNN & image recognition for PID control of microfluidic bubble generation. Created with BioRender.com.

In this study, we use a flow-focusing geometry to produce nitrogen gas (dispersed phase) bubbles in an aqueous phase of 0.5 wt% sodium dodecyl sulfate (SDS) dissolved in DI water (continuous phase). The dispersed phase is injected into the device as pressurized nitrogen gas controlled by a differential pressure controller and the continuous phase is injected by using a differential pressure controller to adjust the pressure in a pressurized liquid reservoir and thus drive flow into the microfluidic device as depicted in Figure 1. All microfluidic devices in this study have undergone hydrophilic-surface treatment to ensure stable formation of gas bubbles using a 2 wt% polyvinyl alcohol (PVA) solution [12].

2.2. Proportional-integral-derivative (PID) control

PID control is one of the most fundamental types of control and is widely used in industrial applications due to its simplicity and effectiveness [28]. It has been widely studied, can address a wide range of process behaviors, and is straightforward to implement, making it a natural choice for control of microfluidics. PID feedback control operates by continuously comparing the desired setpoint to the process output, giving the error, e. The proportional term responds to the current error, the integral term accumulates past errors to eliminate steady-state discrepancies (offset), and the derivative term accounts for the rate of change of the error, as shown in Equation 1.

$$u(t) = K_C e(t) + \frac{K_C}{\tau_I}\int_0^t e(t)dt + K_C \tau_D \frac{de}{dt} + c_s \quad (1)$$

where K_c is the proportional gain, τ_I is the integral time-constant in minutes, τ_D is the derivative time constant in minutes, and c_s is the controller bias (actuating signal when e=0) [28]. These terms are combined to compute the controller output ($u(t)$), aiming to reduce the error and maintain stable and precise control of the process. In this study, two separate control schemes are explored: manipulating the pressure of the dispersed air phase to control microbubble diameter and manipulating the liquid driving pressure of the continuous phase to control microbubble diameter as illustrated in the control scheme of Figure 1.

Altering the PID tuning parameters K_C, τ_I , and τ_D can significantly influence the response of the controller; increasing the proportional gain enhances responsiveness, but may lead to overshooting, while adjusting the integral and derivative time-constants affects the elimination of steady-state error and reduces the settling time, respectively. This method has been used in many applications, but it relies on measuring the process output in real-time. Numerous process parameters, including pressure and temperature, can be measured directly using commercially available real-time in-line sensors. However, microfluidic processes currently lack reliable, industry-proven inline sensor technologies that can directly measure the important process variables that need to be controlled such as size, shape, and flow regime. Thus, we use an artificial intelligence (AI)-based approach to create an indirect sensor, known as a soft-sensor, when controlling microfluidics.

2.3. Soft sensors

When sensor variables are difficult to measure, soft-sensors can be used to estimate them. There are three types of soft-sensor models: knowledge-based models that rely on first principles, black-box models that are data-driven, and hybrid models that combine the two [29]. In this study, a black-box model consisting of a two-step process is used to estimate the flow regime and diameter of the process output, gas bubbles. The first step in our process is using a convolutional neural network (CNN) for image classification. CNNs have played a crucial role in the development and advancement of computer vision and artificial intelligence (AI) [30]. In this study, a linear architecture CNN is used to classify the microfluidic output into one of three regimes: liquid-dominated flow, air-dominated flow, and microbubble flow, as shown in Figure 2. The second step in our process is using a Hough image recognition algorithm for detection of the microbubbles. This algorithm is designed for feature extraction and gives outputs of their location and diameter.

Figure 2. Representative training three flow regimes for CNN: (a) A liquid-dominated flow regime without bubble generation, (b) bubble generation in the dripping regime, and (c) air-dominated jetting regime.

Our novel soft-sensor operates as follows: first, a CNN trained for image classification determines the current flow regime of the process from a snapshot of the device taken by a high-speed microscope camera. When the process is in a bubble producing dripping regime, an image recognition algorithm measures the diameter of the bubbles being produced. The combination of the CNN and image recognition is the soft-sensor output on which the controller acts to match the bubble diameter to the user-specified setpoint. When the process is not in a bubble producing flow regime, a direct controller action is taken to return the process to the production of gas bubbles. Our two-step approach is superior to other microfluidic control techniques because of its ability to return to the bubble-producing dripping regime when a disturbance causes it to move into a flow regime in which bubbles are not being produced. Our controller acts in real-time and can obtain measurements and adjust setpoints with an average sampling frequency of 108 milliseconds.

2.4. Microfluidic fabrication and operation

Photomasks for microfluidic geometries were purchased from Artnet Pro, Inc. Silicon wafers were cleaned with IPA and DI water before oxygen plasma cleaning (Anatech) for enhanced bonding. SU-8 2025 photoresist was spin coated onto the silicon wafer before soft-baking at 65°C for 3 minutes, then at 95°C for 6 minutes. The wafer was exposed to 160 mJ/cm^2 at 365 nm intensity (ABM). After exposure, the wafer was post-baked for 2 minutes at 65°C and then for 6 minutes at 95°C. Lastly, the silicon wafer was gently agitated for 8 minutes in SU-8 developer. PDMS (SYLGARD 184) was mixed in a 10:1 weight ratio of elastomer to curing agent. The mixture was degassed in a vacuum chamber for 1 hour to remove all bubbles before curing for 1 hour in an 80°F oven. The resulting elastomer mold was cut from the master and oxygen plasma bonded to a glass slide. 2 wt% PVA was surface coated onto the PDMS for a hydrophilic coating [12].

The aqueous phase in all experiments was 0.5 wt% SDS dissolved in DI water. The aqueous phase was administered using a differential pressure controller (Alicat) to pressurize a liquid reservoir to drive flow into the device. Compressed nitrogen (Airgas) was used for the dispersed phase and was controlled using a differential pressure controller (Alicat). Images used for the control scheme were taken on a Nikon eclipse TE200 inverted microscope with 3 different high-speed cameras, a Photron Mini AX-200, a Phantom Vision Research v7.3, and a Phantom Vision Research v611 proving the adaptability of this approach across multiple microfluidic setups.

2.5. Neural network architecture and training

A sequential 19-layer CNN was created using the Keras API inside of Tensorflow. The architecture contained 4 convolution layers using 3 x 3 convolutions and 2 x 2 max pooling. The remaining structure was flattened with a dropout layer set at 50%. There were two dense layers, one with rectified linear activation and the final layer with softmax activation function. The neural net was trained with 128 x 600 resolution images. 43,554 images were used for neural net training and the net was validated with an additional 4,839 images. 100% accuracy was achieved for both training and validation sets within 5 epochs as shown in Figure 3.

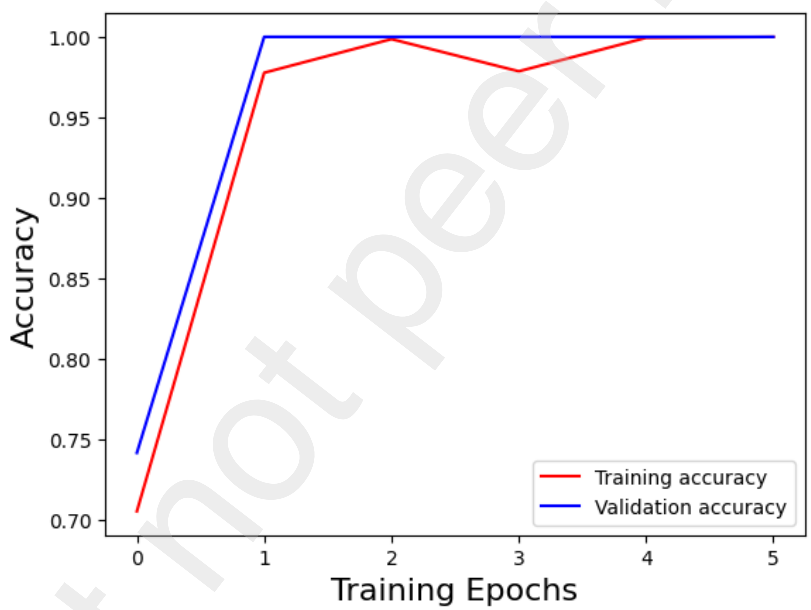

Figure 3. Training and validation accuracy of CNN.

2.6. Image recognition and feature extraction

Image recognition was completed using Matlab image recognition functions. Since the bubbles in this work are circular, the function imfindcircles was used. This built-in function uses a Hough transform to isolate features and extract their location and size. Hough transforms are techniques used in computer vision and image analysis for feature extraction [31]. This is used to measure the size, position, and uniformity of every bubble present in an image as part of the soft-sensor output.

3. Results and Discussion

3.1. Ziegler-Nichols tuning

Tuning the PID control parameters is required to achieve reliable controller responses. In this study, we tune a single-input, single-output (SISO) controller to control the output diameter of bubbles made in a microfluidic device by varying either the air pressure of the dispersed phase, or the liquid driving pressure of the continuous phase. Ziegler-Nichols open-loop response tuning rules are used to acquire initial tuning parameters before adjustments are made to obtain the desired responses. Ziegler-Nichols tuning is appropriate because the system responses exhibit first-order plus dead-time behavior (FOPDT). Tuning parameters are obtained without the controller while monitoring the response to a step change in the manipulated variable. As shown in the process reaction-curve in Figure 4, a tangent line through the inflection point is drawn to estimate the delay time (τ_d) and response time (τ). Here, u is the step change in the process input, such as gas pressure, and y is the change in the measured process variable, which is the bubble diameter herein. These variables are used to calculate controller parameters, where $K_C = 1.2$ $\left(\frac{\tau \Delta u}{\tau_d \Delta y}\right)$, $\tau_I = 2.0\ \tau_d\ and\ \tau_D = 0.5\ \tau_d$ [32]. Small changes in tuning parameters are then made to achieve the desired slightly overdamped response from our controller.

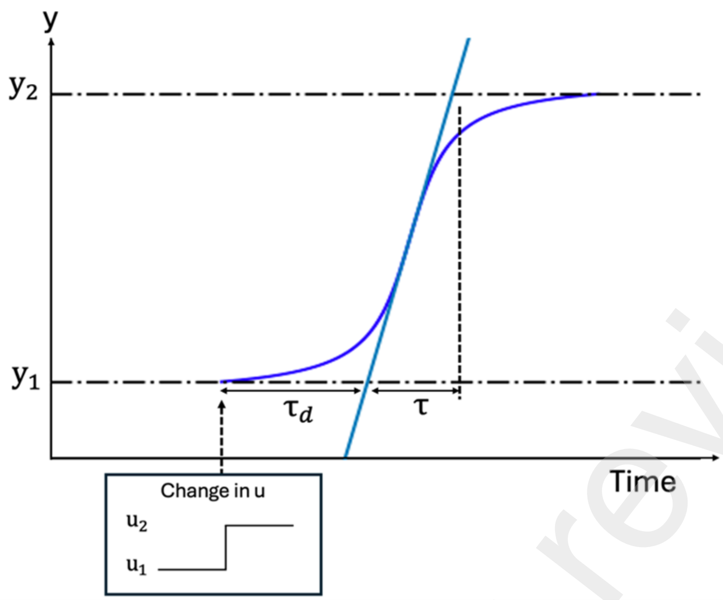

Figure 4. Process reaction curve for a first-order plus dead time (FOPDT) response in the process variable to a step change in the manipulated variable used for Ziegler-Nichols open-loop tuning [31].

For a step pressure increase from 18.7 to 20.3 kPa, an increase in diameter is shown in Figure 5. Plotting the tangent line to the curve, the delay time is 1.1 second and the response time is 1 second. These yield K_C = 0.125 kPa/μm, $\tau_I =$ 2.2 seconds, and $\tau_D =$ 0.55 seconds.

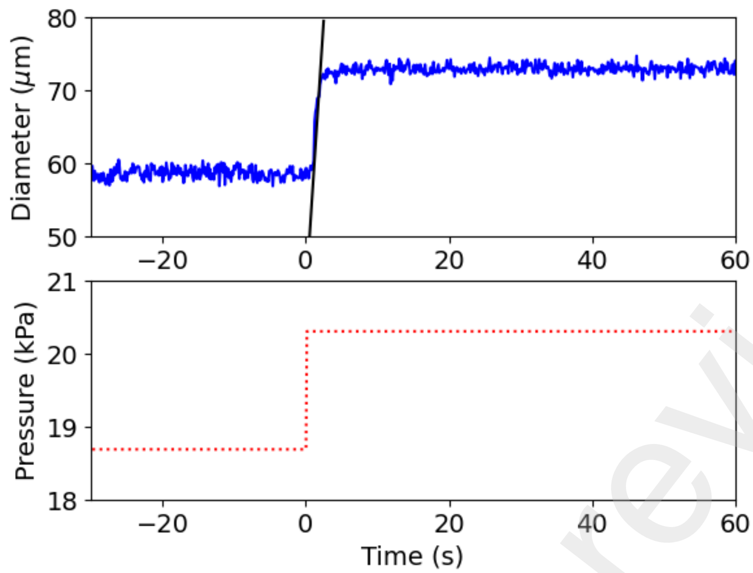

Figure 5. Diameter response (a) from open-loop step change in pressure from 18.7 kPa to 20.3 kPa (b) using Ziegler-Nichols tuning.

Instead of the gas pressure, the flowrate of the continuous phase is manipulated by varying the liquid driving pressure. For a driving pressure step change from 31.7 kPa to 29.6 kPa, the delay time is 1.2 seconds, and the response time is 2.3 seconds, yielding K_C = -0.21 kPa/μm, $\tau_I = 2.4$ seconds, and $\tau_D = 0.6$ seconds, as shown in Figure 6.

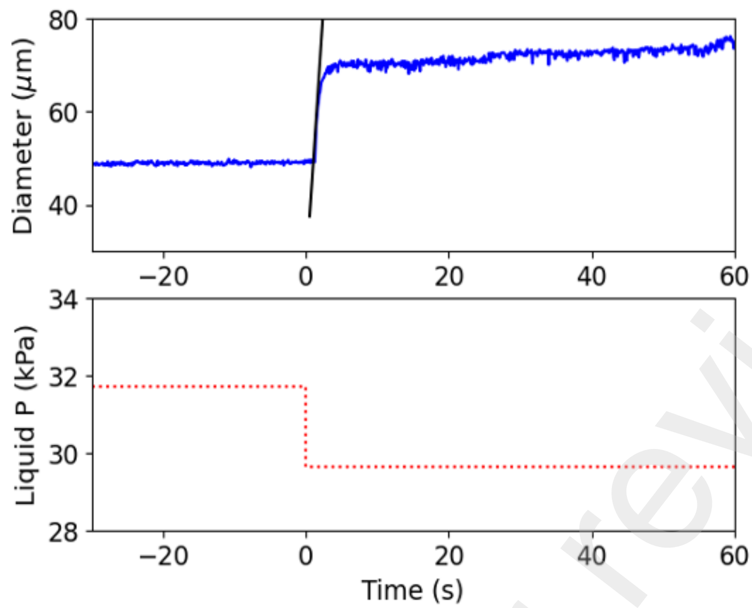

Figure 6. Diameter response (a) from open-loop step change in flowrate created by a step change in liquid pressure from 31.7 kPa to 29.6 kPa (b) using Ziegler-Nichols tuning.

3.2. Setpoint Tracking

Setpoint tracking by PID control holds significant importance in optimizing process performance, ensuring close adherence to desired operating conditions and allowing for switches to new operating setpoints. For many microfluidic processes, effective changes in bubble/droplet diameters are required for different applications. For example, the gas bubble diameter is crucial in determining its resonance frequency, particularly in applications where bubbles serve as a contrast agent in ultrasound sonography [33]. In the context of microfluidic reactors, the droplet diameter plays a crucial role in influencing the reaction rates and kinetics of associated chemical processes [34].

With our controller, we can dynamically manipulate either the continuous phase (aqueous flowrate via liquid driving pressure), or the dispersed phase (air pressure) to reach a desired setpoint, output bubble diameter. Figures 7-10 show the experimental controller actions after a diameter setpoint changes at time zero. Each color represents a different setpoint change: dashed lines for setpoint changes, and solid lines for process variable changes. The liquid driving pressure (aqueous flowrate) is kept constant, and the air pressure is manipulated by the controller to reach the new setpoint in Figures 7 and 8, where the first shows the response for an increase in the diameter setpoint and the latter for a decrease in the diameter setpoint. Both responses are adjusted to be slightly overdamped; that is, having small overshoot before settling to the desired value, with all responses settling to the new setpoint in under 100 seconds – similar to those in other microfluidic control studies [20]. This response is more reliable compared to underdamped systems having large oscillations in diameter and long settling times. Underdamped tuning parameter responses are shown in Figures S1 and S2.

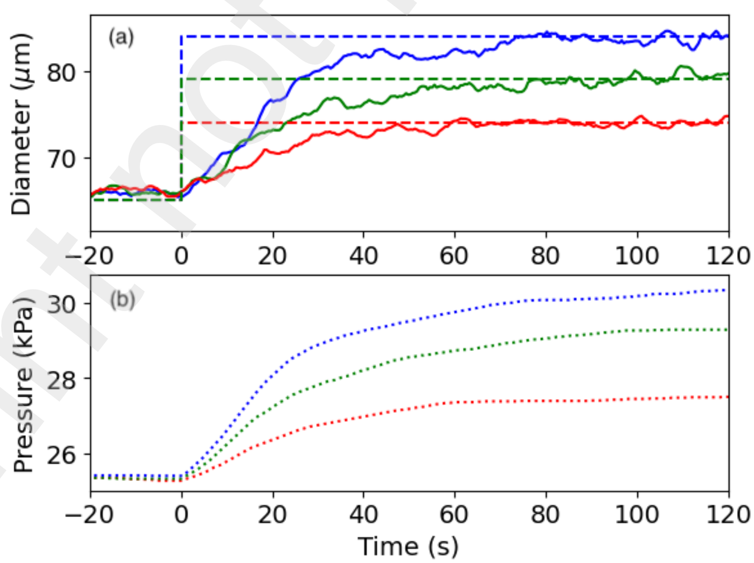

Figure 7. Setpoint tracking diameter responses (a) while varying pressure (b) while at constant aqueous flowrate for increases in diameter setpoint.

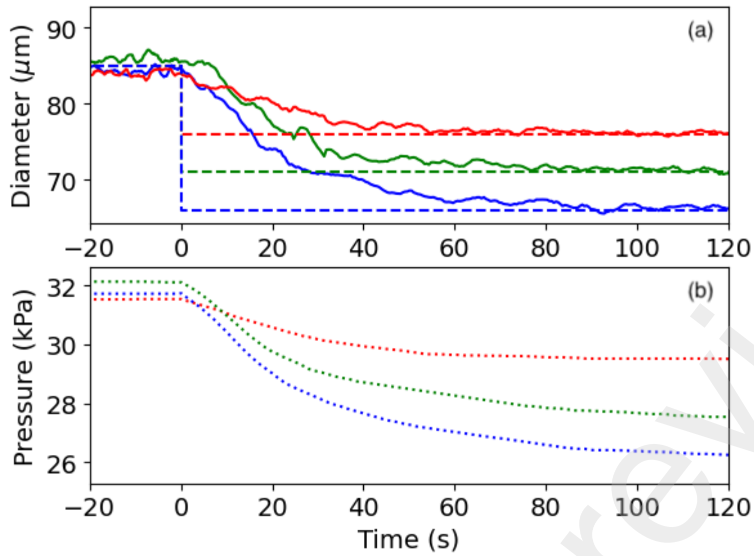

Figure 8. Setpoint tracking diameter responses (a) while varying pressure (b) while at constant aqueous flowrate for decreases in diameter setpoint.

We also perform tests with constant pressure while manipulating the aqueous flowrate via liquid driving pressure to achieve the new setpoint as shown in Figures 9 and 10. The controller can achieve changes in setpoint for increases in diameter as shown in Figure 9 and for decreases in diameter as shown in Figure 10. Again, these responses are overdamped, not allowing any overshoot, and it is seen that response times are considerably faster using pressure driven flow for the aqueous phase than widely used commercially available syringe pumps seen in Figures S3 and S4.

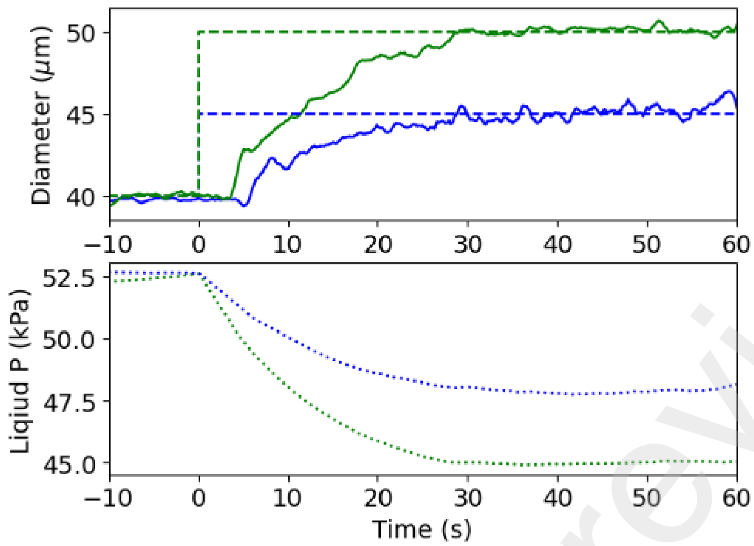

Figure 9. Setpoint tracking diameter responses (a) while varying liquid driving pressure (b) while at constant air pressure for increases in diameter setpoint.

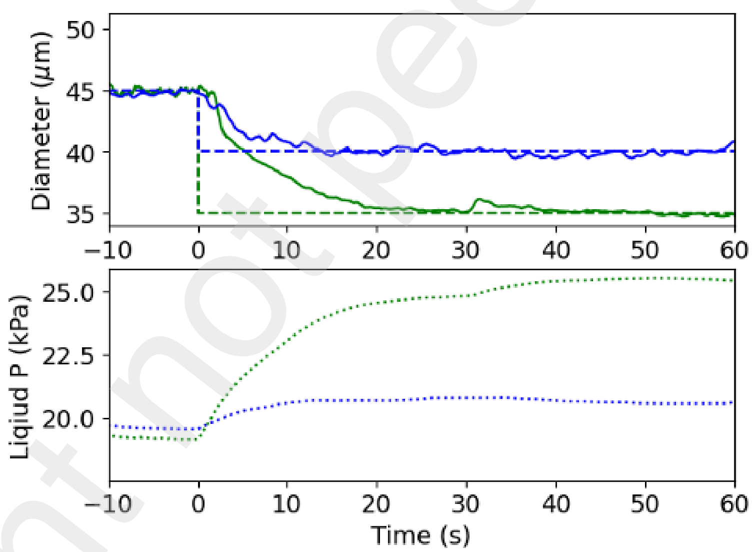

Figure 10. Setpoint tracking diameter responses (a) while varying liquid driving pressure (b) while at constant air pressure for decreases in diameter setpoint.

3.3. Disturbance Rejection

Disturbance rejection is needed to overcome all potential disruptions during process operation. This is especially important in intricate microfluidic processes in which minute variations can have large impacts on the process outputs due to inherently-small length scales. Such disturbances in microbubble production occur due to changes in air pressure, aqueous phase flowrate, fouling, clogging, changes in wetting properties, and external factors that cannot be anticipated [11,12,14]. For example, a random physical vibration such as one produced by motion of a person near the microfluidic set-up can significantly impact the uniformity of the resulting bubbles.

Our control system is superior to many microfluidic controllers because its CNN architecture allows it to recover from sharp disturbances that would otherwise move to non-bubble generating flow regimes, as shown in Figures 11 and 12. In Figure 12a, there are no bubbles being produced at a pressure of 29.3 kPa, so the controller linearly increases the pressure until bubbles are generated and the controller obtains an error for PID diameter control. The onset of bubble production occurs 21.5 seconds later at a breakthrough pressure of 41.9 kPa shown in Figure 12b. Now that bubbles are being produced and the controller can measure an error, PID control takes over and reduces the pressure to 35.7 kPa to reach the intended setpoint shown in Figure 12c. Basic PID control cannot achieve this transition to bubble creation because without bubbles, there is no way to obtain the current error. A recovery of flow regime video is shown in Video S5. Although neural networks for microfluidics control have been reported, their controllers are trained in the bubble generating regime only and do not account for the complex nature of bubble breakup at elevated pressures or flowrates often needed to achieve breakthrough and induce breakup [16].

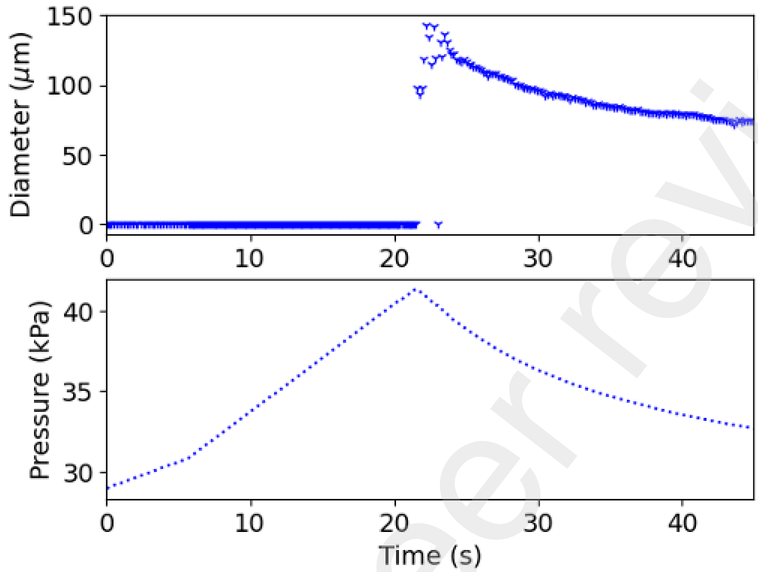

Figure 11. Diameter responses (a) while varying air pressure (b) to overcome liquid-dominated flow by reaching the breakthrough pressure of 41.9 kPa and tapering down to 35.7 kPa to achieve a setpoint of 70 μm corresponding to images in Figure 12. Diameter values of zero indicate no bubbles production.

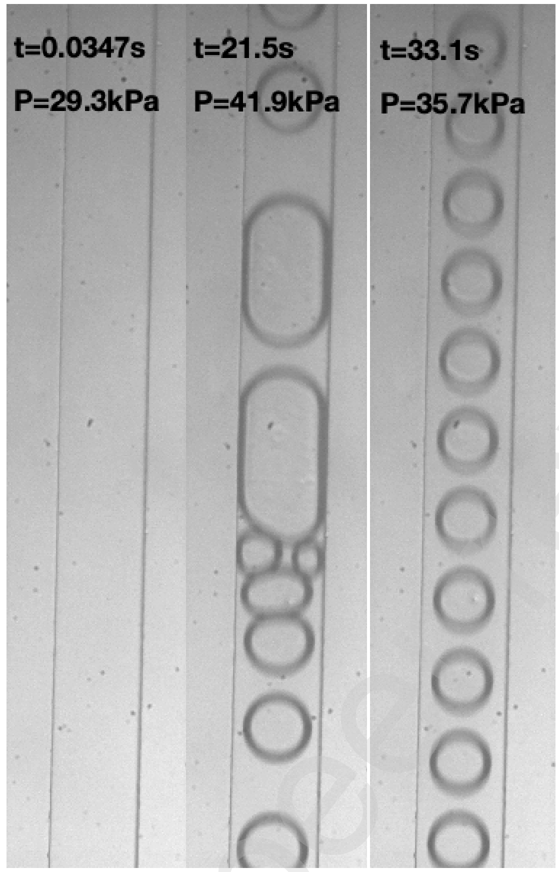

(a) (b) (c)

Figure 12. Time series response to sharp disturbance knocking flow out of a bubble producing flow regime. (a) System that has been disturbed and is in a liquid dominated flow regime – no longer producing bubbles. (b) Moment breakthrough pressure is reached by CNN allowing bubbles to be produced. (c) Controller continued to reduce the pressure from the breakthrough pressure to reach the setpoint diameter of 70 μm.

To track the CNN's activation frequency in disturbance recovery, a one-hour test is conducted at a constant setpoint, beginning with a dispersed phase pressure of 0 kPa. The CNN increases the pressure to initiate bubble production, after which PID control maintains the setpoint. The CNN activates if disturbances push the system into liquid- or air-dominated flow regimes. Over the hour, PID control maintained the setpoint 99.2% of the time, but the CNN's disturbance recovery is crucial for sustained bubble production, as shown in Figure S6. This experiment demonstrates the controller's ability to start from a zero pressure condition using the CNN to drive the pressure up into the bubble production regime.

In addition to large disturbances, our controller overcomes disturbances small enough to create error only in the bubble diameter. As mentioned, two separate control schemes can be employed: altering dispersed phase pressure to regain the setpoint after a disturbance in flowrate as shown in Figure 13 and manipulating flowrate by changing liquid driving pressure to maintain setpoint after a disturbance in pressure as shown in Figure 14. The former shows a slightly overdamped response as the pressure slowly decreases without overshoot to regain the diameter setpoint after the flowrate disturbance. The pressure response is able to regain the setpoint in under 20 seconds. The latter is also a slightly overdamped response to return the diameter to the setpoint following a sharp increase in dispersed phase pressure that causes the diameter to increase quickly above the setpoint. The controller increases the liquid driving pressure and thus the aqueous flowrate returns the bubbles to the setpoint in only 20 seconds.

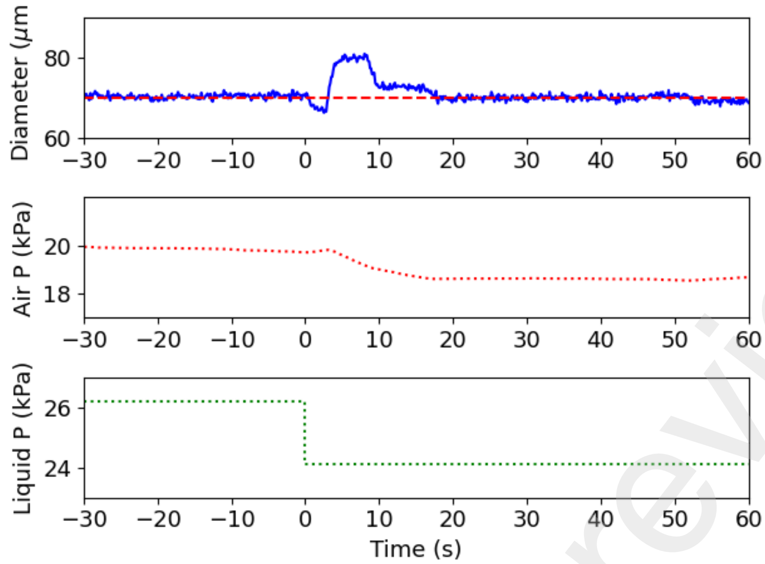

Figure 13. Diameter response (a) to maintain the setpoint value by varying the air pressure (b) to overcome a flowrate disturbance caused by a change in liquid driving pressure (c).

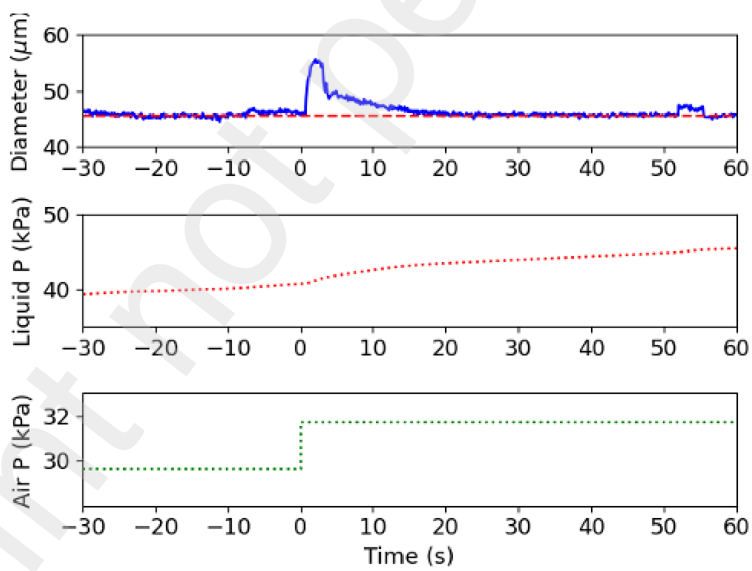

Figure 14. Diameter response (a) to maintain the setpoint value by varying the liquid driving pressure (c) to overcome an air pressure disturbance (b).

Another important aspect of disturbance rejection is the ability to remain stable for long periods of time. A typical operating shift in manufacturing industries in the US and many countries is eight hours [35] during which many changes in operating conditions can occur. Figure 15 shows performance of a gas bubble generation process left unattended without control measures (i.e., the flowrate and the pressure are kept constant). Over extended durations, frequent disruptions in flow conditions lead to significant variations in the output bubble size. Remarkably, only 2.16% of the produced bubbles fall within 5% of the initial bubble diameter. The exact cause of these disruptions is unknown, necessitating the implementation of a control system to counteract them, as they cannot be systematically eliminated from the process.

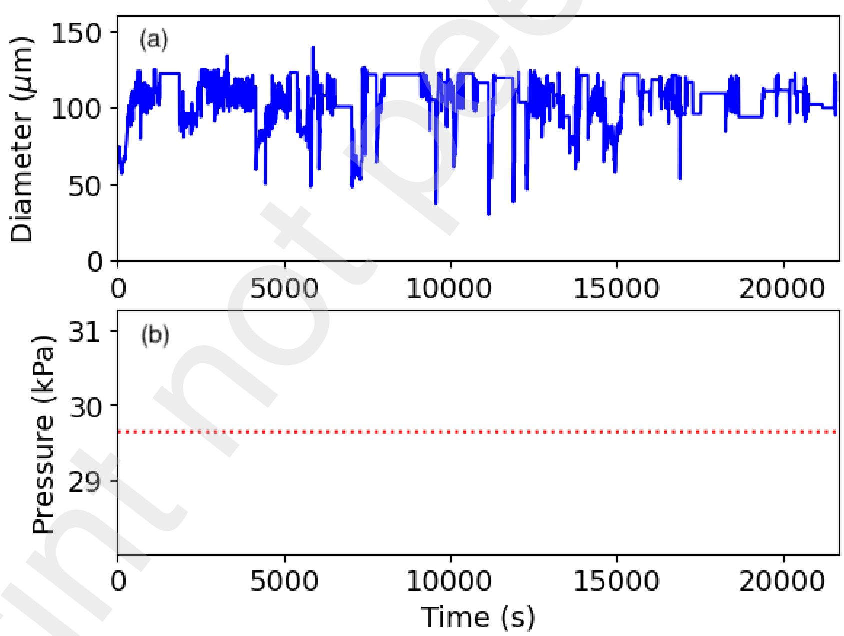

Figure 15. Long-term diameter response (a) of an open-loop control system with constant air pressure (b) at constant aqueous flowrate.

This drastic variability is avoided with control action, as shown in Figure 16. Despite disturbances, the controller adjusts the pressure to maintain the setpoint. Throughout the eight-hour period, our controller achieved 99.2% accuracy, with bubbles deviating by no more than 5% from the setpoint. Notably, the pressure required to satisfy the setpoint must be increased gradually by over 50%; while we do not fully understand the physical origin of such an adjustment in the pressure, this result nevertheless highlights the importance of feedback control to enable stable and robust microfluidic manufacturing.

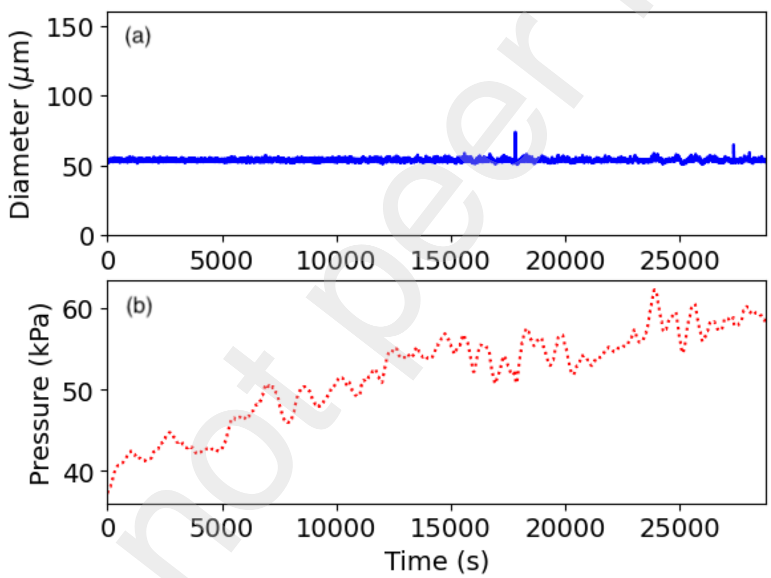

Figure 16. Long-term diameter response (a) of a closed-loop control system with varying air pressure (b) at constant aqueous flowrate.

4. Conclusions

Microfluidic devices offer precise control for producing droplets and bubbles crucial for various industries. Transitioning from laboratory to industrial-scale operations poses challenges presented by disturbances, fouling, and changes in device performance. These necessitate continuous monitoring and adjustments to manipulated variables that maintain user-specified setpoints. The integrating feedback controllers herein enhance product uniformity and reduce the labor-intensive tasks associated with process maintenance, addressing a critical need in scaling-up microfluidic processes for industrial applications. Our experimental results show that PID control is a resilient feedback control mechanism, relying on a soft-sensor to obtain error measurements using artificial intelligence in the face of unreliable physical measurements. Our CNN-driven, soft-sensor identifies flow regimes enabling the controller to regain bubble-producing flow regimes when shifted by disturbances to undesired regimes. In addition to self-recovery, our controller reduces errors while maintaining setpoints, countering disturbances, and stabilizing operation over long times. Our controller permits over 99% of bubbles produced during 8-hours to fall within 5% of setpoint diameters; in contrast to only 2.16% when control action is not implemented. Leveraging a combination of machine learning and image recognition software, soft-sensors herein enable feedback control in droplet-based microfluidic systems, potentially enhancing control over the size, shape, and functionality of microfluidic-generated emulsions.

CRediT authorship contribution statement

Owen Land: Writing – review and editing, Writing – original draft, Conceptualization, Data curation, Funding acquisition, Investigation, Methodology, Software, Validation, Visualization, Formal analysis **Warren Seider**: Writing – review and editing, Supervision, Project administration, Methodology, Funding acquisition, Conceptualization, Formal analysis **Daeyeon Lee**: Writing – review and editing, Supervision, Project administration, Methodology, Funding acquisition, Conceptualization, Formal analysis, Resources

Declaration of competing interest

Daeyeon Lee is a co-founder of InfiniFluidics.

Data availability

Data will be made available on request.

Declaration of generative AI and AI-assisted technologies in the writing process

During the preparation of this work the author(s) used OpenAI's ChatGPT to produce code for creation and training of neural network models. After using this tool/service, the author(s) reviewed and edited the content as needed and take(s) full responsibility for the content of the published article.

Acknowledgments

This work was supported by the National Science Foundation Research Traineeship (NRT) Program - Interdisciplinary Training in Data Driven Soft Materials Research and Science Policy – Grant No. 2152205.

Appendix A. Supplementary data

Supplementary data to this article can be found online at

References

[1] M.I. Hajam, M.M. Khan, Microfluidics: a concise review of the history, principles, design, applications, and future outlook, Biomater. Sci. 12 (2024) 218–251. https://doi.org/10.1039/D3BM01463K.

[2] A.J. deMello, Control and detection of chemical reactions in microfluidic systems, Nature 442 (2006) 394–402. https://doi.org/10.1038/nature05062.

[3] K.S. Elvira, X.C. i Solvas, R.C.R. Wootton, A.J. deMello, The past, present and potential for microfluidic reactor technology in chemical synthesis, Nature Chem 5 (2013) 905–915. https://doi.org/10.1038/nchem.1753.

[4] H.K. Bui, K.Y. Kim, H. Kim, J.-P. Ahn, T. Yu, T.S. Seo, Total Integration of the Sample Injection, Microdroplet Reaction, Phase Separation, Real-Time Optical Detection, and Recovery of Diverse Silver–Gold Bimetallic Nanoalloys in a Continuous Process, Particle & Particle Systems Characterization 38 (2021) 2000244. https://doi.org/10.1002/ppsc.202000244.

[5] S.D. Ling, Y. Geng, A. Chen, Y. Du, J. Xu, Enhanced single-cell encapsulation in microfluidic devices: From droplet generation to single-cell analysis, Biomicrofluidics 14 (2020) 061508. https://doi.org/10.1063/5.0018785.

[6] Z. Wang, A.S. Huang, L. Tang, J. Wang, G. Wang, Microfluidic-assisted single-cell RNA sequencing facilitates the development of neutralizing monoclonal antibodies against SARS-CoV-2, Lab Chip 24 (2024) 642–657. https://doi.org/10.1039/D3LC00749A.

[7] A. Reece, B. Xia, Z. Jiang, B. Noren, R. McBride, J. Oakey, Microfluidic techniques for high throughput single cell analysis, Current Opinion in Biotechnology 40 (2016) 90–96. https://doi.org/10.1016/j.copbio.2016.02.015.

[8] L. Shang, Y. Cheng, Y. Zhao, Emerging Droplet Microfluidics, Chem. Rev. 117 (2017) 7964–8040. https://doi.org/10.1021/acs.chemrev.6b00848.

[9] S. Damiati, U.B. Kompella, S.A. Damiati, R. Kodzius, Microfluidic Devices for Drug Delivery Systems and Drug Screening, Genes (Basel) 9 (2018) 103. https://doi.org/10.3390/genes9020103.

[10] S. Mehraji, D.L. DeVoe, Microfluidic synthesis of lipid-based nanoparticles for drug delivery: recent advances and opportunities, Lab Chip 24 (2024) 1154–1174. https://doi.org/10.1039/D3LC00821E.

[11] C. Duchêne, V. Filipe, S. Huille, A. Lindner, Clogging of microfluidic constrictions by monoclonal antibody aggregates: role of aggregate shape and deformability, Soft Matter 16 (2020) 921–928. https://doi.org/10.1039/C9SM01583C.

[12] T. Trantidou, Y. Elani, E. Parsons, O. Ces, Hydrophilic surface modification of PDMS for droplet microfluidics using a simple, quick, and robust method via PVA deposition, Microsyst Nanoeng 3 (2017) 1–9. https://doi.org/10.1038/micronano.2016.91.

[13] E.J. Kappert, M.J.T. Raaijmakers, K. Tempelman, F.P. Cuperus, W. Ogieglo, N.E. Benes, Swelling of 9 polymers commonly employed for solvent-resistant nanofiltration membranes: A comprehensive dataset, Journal of Membrane Science 569 (2019) 177–199. https://doi.org/10.1016/j.memsci.2018.09.059.

[14] M. Armani, Z. Cummins, J. Gong, P. Mathai, R. Probst, C. Ropp, E. Waks, S. Walker, B. Shapiro, Feedback Control of Microflows, in: J.J. Gorman, B. Shapiro (Eds.), Feedback Control of MEMS to Atoms, Springer US, New York, NY, 2012: pp. 269–319. https://doi.org/10.1007/978-1-4419-5832-7_9.

[15] O.J. Dressler, P.D. Howes, J. Choo, A.J. deMello, Reinforcement Learning for Dynamic Microfluidic Control, ACS Omega 3 (2018) 10084–10091. https://doi.org/10.1021/acsomega.8b01485.
[16] P. Hadikhani, N. Borhani, S.M. H. Hashemi, D. Psaltis, Learning from droplet flows in microfluidic channels using deep neural networks, Sci Rep 9 (2019) 8114. https://doi.org/10.1038/s41598-019-44556-x.
[17] X. Duan, Z. Zheng, Y. Luo, C. Song, Closed-loop feedback control for droplet-based microfluidics: a characteristic investigation on passive and on-demand droplet generation, in: International Conference on Optical and Photonic Engineering (icOPEN 2022), SPIE, 2023: pp. 196–201. https://doi.org/10.1117/12.2666602.
[18] Y. Xie, A.J. Dixon, J.M.R. Rickel, A.L. Klibanov, J.A. Hossack, Closed-loop feedback control of microbubble diameter from a flow-focusing microfluidic device, Biomicrofluidics 14 (2020) 034101. https://doi.org/10.1063/5.0005205.
[19] E. Miller, M. Rotea, J.P. Rothstein, Microfluidic device incorporating closed loop feedback control for uniform and tunable production of micro-droplets, Lab Chip 10 (2010) 1293–1301. https://doi.org/10.1039/B925497H.
[20] Smart Microfluidics - Fluigent, (n.d.). https://www.fluigent.com/ (accessed January 30, 2024).
[21] OB1 Mk3+ Flow Controller, Darwin Microfluidics (n.d.). https://darwin-microfluidics.com/products/ob1-mk3-flow-controller (accessed February 8, 2024).
[22] W. Zeng, S. Li, Z. Wang, Characterization of syringe-pump-driven versus pressure-driven microfluidic flows, in: 2015 International Conference on Fluid Power and Mechatronics (FPM), 2015: pp. 711–715. https://doi.org/10.1109/FPM.2015.7337207.
[23] A.M. Gañán-Calvo, J.M. Gordillo, Perfectly Monodisperse Microbubbling by Capillary Flow Focusing, Phys. Rev. Lett. 87 (2001) 274501. https://doi.org/10.1103/PhysRevLett.87.274501.
[24] S.L. Anna, N. Bontoux, H.A. Stone, Formation of dispersions using “flow focusing” in microchannels, Applied Physics Letters 82 (2003) 364–366. https://doi.org/10.1063/1.1537519.
[25] J. Wu, S. Yadavali, D. Lee, D.A. Issadore, Scaling up the throughput of microfluidic droplet-based materials synthesis: A review of recent progress and outlook, Applied Physics Reviews 8 (2021) 031304. https://doi.org/10.1063/5.0049897.
[26] A.S. Utada, A. Fernandez-Nieves, H.A. Stone, D.A. Weitz, Dripping to Jetting Transitions in Coflowing Liquid Streams, Phys. Rev. Lett. 99 (2007) 094502. https://doi.org/10.1103/PhysRevLett.99.094502.
[27] A.S. Utada, L.Y. Chu, A. Fernandez-Nieves, D.R. Link, C. Holtze, D.A. Weitz, Dripping, Jetting, Drops, and Wetting: The Magic of Microfluidics, MRS Bulletin 32 (2007) 702–708. https://doi.org/10.1557/mrs2007.145.
[28] G. Stephanopoulos, Chemical Process Control: An Introduction to Theory and Practice, 3rd ed., Pearson, 1984.
[29] V. Brunner, M. Siegl, D. Geier, T. Becker, Challenges in the Development of Soft Sensors for Bioprocesses: A Critical Review, Frontiers in Bioengineering and Biotechnology 9 (2021). https://www.frontiersin.org/articles/10.3389/fbioe.2021.722202 (accessed January 11, 2024).
[30] L. Alzubaidi, J. Zhang, A.J. Humaidi, A. Al-Dujaili, Y. Duan, O. Al-Shamma, J. Santamaría, M.A. Fadhel, M. Al-Amidie, L. Farhan, Review of deep learning: concepts,

CNN architectures, challenges, applications, future directions, Journal of Big Data 8 (2021) 53. https://doi.org/10.1186/s40537-021-00444-8.
[31] T. Ferguson, D. Baker, Feature Extraction Using the Hough Transform, in: 2002. https://www.semanticscholar.org/paper/Feature-Extraction-Using-the-Hough-Transform-Ferguson-Baker/ea0cdf30a4d2c915c5008c97dbdeaed6cdff5e55 (accessed January 11, 2024).
[32] Open Loop Tuning, (n.d.). https://www.homepages.ed.ac.uk/jwp/control06/controlcourse/course/map/ZN/opennotes.html (accessed January 11, 2024).
[33] J.J. Choi, J.A. Feshitan, B. Baseri, S. Wang, Y.-S. Tung, M.A. Borden, E.E. Konofagou, Microbubble-size dependence of focused ultrasound-induced blood-brain barrier opening in mice in vivo, IEEE Trans Biomed Eng 57 (2010) 145–154. https://doi.org/10.1109/TBME.2009.2034533.
[34] S.H. Al-Mutairi, H.A. Nasr-El-Din, A.D. Hill, A.D. Al-Aamri, Effect of Droplet Size on the Reaction Kinetics of Emulsified Acid With Calcite, SPE Journal 14 (2009) 606–616. https://doi.org/10.2118/112454-PA.
[35] Average Workweek by Country 2023, Wisevoter (n.d.). https://wisevoter.com/country-rankings/average-workweek-by-country/ (accessed February 14, 2024).